

## Time-dependent degradation of Pt/ZnO nanoneedle rectifying contact based piezoelectric nanogenerator

C. Periasamy and P. Chakrabarti

Citation: *J. Appl. Phys.* **109**, 054306 (2011); doi: 10.1063/1.3553862

View online: <http://dx.doi.org/10.1063/1.3553862>

View Table of Contents: <http://jap.aip.org/resource/1/JAPIAU/v109/i5>

Published by the [American Institute of Physics](#).

---

### Related Articles

Optimum drift velocity for single molecule fluorescence bursts in micro/nano-fluidic channels

*Appl. Phys. Lett.* **101**, 043120 (2012)

Incorporation of the stress concentration slots into the flexures for a high-performance microaccelerometer

*Rev. Sci. Instrum.* **83**, 075002 (2012)

Finite element analysis of scaling of silicon micro-thermoelectric generators to nanowire dimensions

*J. Renewable Sustainable Energy* **4**, 043110 (2012)

Self-assembled synthesis and characterization of microchannels in polymeric membranes

*J. Appl. Phys.* **112**, 024701 (2012)

Fast electrothermally activated micro-positioner using a high-aspect-ratio micro-machined polymeric composite

*Appl. Phys. Lett.* **101**, 033108 (2012)

---

### Additional information on J. Appl. Phys.

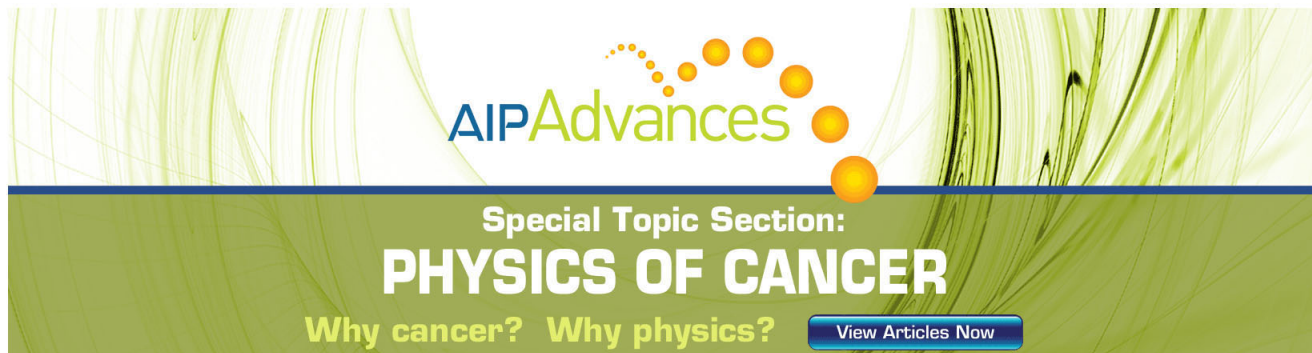
Journal Homepage: <http://jap.aip.org/>

Journal Information: [http://jap.aip.org/about/about\\_the\\_journal](http://jap.aip.org/about/about_the_journal)

Top downloads: [http://jap.aip.org/features/most\\_downloaded](http://jap.aip.org/features/most_downloaded)

Information for Authors: <http://jap.aip.org/authors>

## ADVERTISEMENT



**AIPAdvances**

Special Topic Section:  
**PHYSICS OF CANCER**

Why cancer? Why physics? [View Articles Now](#)

# Time-dependent degradation of Pt/ZnO nanoneedle rectifying contact based piezoelectric nanogenerator

C. Periasamy and P. Chakrabarti<sup>a)</sup>

*Centre for Research in Microelectronics, Department of Electronics Engineering, Institute of Technology, Banaras Hindu University, Varanasi 221-005, India*

(Received 14 September 2010; accepted 8 January 2011; published online 10 March 2011)

A piezoelectric nanogenerator based on the platinum rectifying contact on ZnO nanoneedle arrays (NNA) has been successfully fabricated on silicon substrate by using the thermal evaporation deposition technique. It is demonstrated that the rectifying platinum contact on ZnO NNA can efficiently convert nanoscale mechanical energy into electrical energy by exploiting the piezoelectric and semiconducting properties of ZnO. The effect of key parameters such as scanning speed, force on scanning tip, and tip abrasion on the nanogenerator has been studied along with long-time stability of the piezoelectric nanogenerator. The study reveals that the nanogenerator output degrades with time primarily due to degradation of the rectifying contact with time and abrasion of the tip caused by repeated scanning. The results of the study are expected to provide quantitative ideas about the long-time stability of ZnO NN based nanogenerators. © 2011 American Institute of Physics. [doi:10.1063/1.3553862]

## I. INTRODUCTION

The miniaturization of a system involving nanoscale devices is highly constrained by the size of traditional batteries. The recharging/replacement of batteries in wireless nanosensors are an additional constraint imposed on their widespread use. Therefore development of a nanoscale power generating device for converting the available form of energy from the environment into electric energy will effectively reduce the size of nanodevices.<sup>1-5</sup> This kind of self power generation mechanism can be used to develop a battery-less smart system for future applications.<sup>1-10</sup> ZnO thin films in the form of nanowire (NW)<sup>11</sup>/nanorod (NR)<sup>12</sup> or nanoneedle (NN) arrays<sup>13,14</sup> constitute a family of one dimensional nanostructures, which find applications in the design of nanopiezoelectronic devices, such as a piezoelectric diode,<sup>15</sup> piezoelectric field-effect-transistor,<sup>16</sup> and piezoelectric-nanogenerator.<sup>17</sup> The strong piezoelectric properties of ZnO are attributed to the absence of a center of symmetry in its wurtzite structural form and a large electromechanical coupling.<sup>11</sup> ZnO nanostructures can efficiently convert nanoscale mechanical energy into electricity by utilizing its coupled effect of piezoelectric and semiconducting properties.<sup>11</sup> The piezoelectric properties of ZnO are utilized to create an electric potential of ionic charges from the elastic deformation of the film. The semiconducting property is subsequently exploited to extract and maintain the charges via a Schottky contact at the metal-ZnO interface. It is further established that ZnO nanostructures have a longer piezoelectric constant than bulk ZnO. Recently, nanogenerators involving a piezoelectric n-type and p-type ZnO nanowire (NW) array have been demonstrated.<sup>17-20</sup> The potential applications of nanogenerators are highly

constrained by their low power output and poor long-term stability. Attempts have been made to improve the situation by involving different mechanical and physical designs of nanogenerators by making use of other materials.<sup>6</sup> The available output from ZnO based nanogenerator degrades significantly in the long run. The long-term stability of a ZnO based nanogenerator and the influence of other key parameters such as general wear and tear of the ZnO nanowire/nanoneedles, tip abrasion, normal tip force, etc. have not been studied systematically so far. Therefore an investigation and understanding of the piezoelectric as well mechanical properties of ZnO nanostructures is important for their potential application in the field of energy science. This paper demonstrates a simple technique for fabrication of piezoelectric nanogenerator based on ZnO nanoneedle arrays (NNAs) for self powering nanodevices. An array of aligned ZnO nanoneedles on a Si substrate has been successfully developed in our laboratory by using the inexpensive vacuum deposition technique. The thin film NNA was subsequently tested for its potential to generate power in the form of electrical pulses that can be used for driving nanodevices. The detailed piezoelectric charging/discharging process of the array of ZnO NN is studied by examining individual nanoneedle using conductive atomic force microscope (CAFM). Also we report the long-term stability of ZnO based nanogenerator fabricated by the vacuum deposition technique along with the influence of different key parameters on the performance of the nanogenerator.

## II. EXPERIMENTAL DETAILS

The samples ZnO nanoneedle arrays were synthesized on a p-type  $\langle 100 \rangle$  silicon substrate by using thermal evaporation deposition technique. Ultrapure ZnO powder (99.99%) from MERK-Chemical Limited, Mumbai, India was used as the source material. Before deposition, the silicon (Si) wafer

<sup>a)</sup>Author to whom correspondence should be addressed. Electronic mail: pchakra@bhu.ac.in.

was first cleaned in sequence with acetone, isopropyl alcohol, and de-ionized (DI) water. The DI water (resistivity,  $\sim 18 \text{ M}\Omega\text{cm}$ ) was obtained from the Milli-Q water plant of Millipore, USA. A 20 nm thick layer of Al doped ZnO (AZO) with  $\sim 1\%$  Al was deposited as a seed layer on silicon wafer using thermal evaporation deposition technique before growing ZnO nanoneedles. The buffer seed layer facilitates subsequent growth of nanoneedles and controls the growth orientation.<sup>21</sup> The thermal deposition setup unit (Model No. 12A4D of HINDVAC, India) was used for growing the layers of AZO and ZnO in sequence. The base pressure of the vacuum chamber was maintained at  $10^{-3}$  mPa. The dc power was set to 45 W, and the evaporation time was set at 40 min. The distance between the substrate to the source was fixed at 18 cm. The substrate was kept at room temperature (300 K) during the deposition of the films. The heating filament used was a conventional molybdenum boat. The appropriate amount (by weight) of ZnO and Al powders were thoroughly mixed with polyvinyl alcohol (PVA) for about 1 h by using agate mortar and pestle sets. Finally the ZnO and Al doped ZnO pellets were prepared with the help of a hot pressure setup. AZO/ZnO pellets were fed to a molebotunim boat and then evaporated by electrical heading for deposition of the films. The in-built digital crystal thickness monitor was set appropriately to the desired value for monitoring the film thickness. The thickness of ZnO thin film layer measured approximately 300 nm. To improve the quality of ZnO thin film nanoneedles and their conductivity, the film was subjected to rapid thermal annealing (RTA) after deposition at a selected temperature (600 °C) in Ar and O<sub>2</sub> environment of a RTA chamber.<sup>22,23</sup> The studies on structural and morphological properties of ZnO thin films were carried out after bringing the temperature down to room temperature (27 °C). The morphology and crystal structures of the samples were characterized with AFM (Model No. SolverPRO-47 from NT-MDT Co., Russia) and XRD (18 KW Cu-rotating anode based x-ray diffractometer, Mode No.: D/MAX, 2500-PC, Rigaku, Japan). Surface morphology and energy-dispersive X-ray analyses were carried out by EDX facility available with the ZEISS SUPRA-40 model SEM system.

### III. RESULTS AND DISCUSSION

#### A. Structural study

Figure 1(a) shows an AFM image of a typical sample of the ZnO nanoneedle array. It reveals that the nanoneedles are uniform and grown vertically from the substrate. The AFM images also clearly demonstrate that a well-aligned closely packed vertical ZnO nanoneedle array with excellent morphology can be grown on silicon substrate with a thin Al doped ZnO (AZO) buffer layer by thermal evaporation method. The average roughness was about 1 nm for a scanning area of  $5 \times 5 \mu\text{m}$ . The x-ray diffraction (XRD) measurement was subsequently carried out to examine the crystal structure of the samples. The XRD spectrum of a typical ZnO film sample grown by the process is shown in Fig. 1(b). The strong (002) peak around  $2\theta = 34.41^\circ$  in the XRD

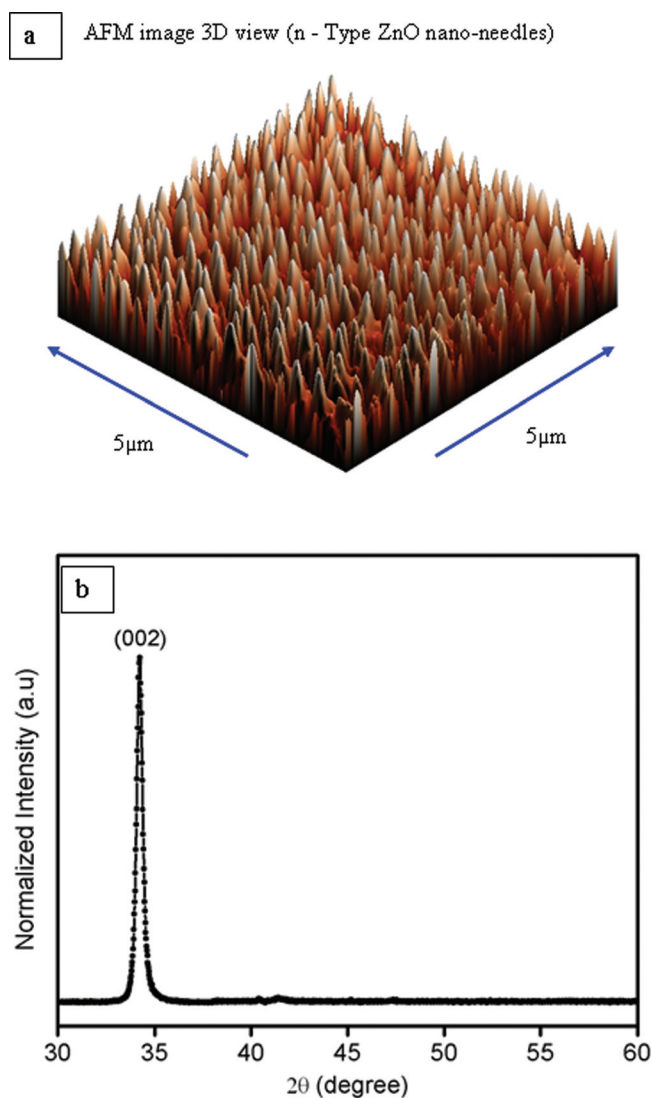


FIG. 1. (Color online) Illustrations of morphological and structural characteristics of *n*-type ZnO NN arrays on Si substrate. (a) AFM image, (b) XRD spectrum.

pattern confirms the *c*-axis orientation perpendicular to the plane of substrate. It further indicates that the ZnO film has a hexagonal wurtzite configuration with a good single crystalline structure.<sup>24</sup> This finding is consistent with our results obtained from AFM studies [Fig. 1(a)]. The XRD results, however, could not detect the presence of Al in the AZO layer. This is attributed to the limited resolution of our existing XRD system and low concentration of Al in AZO. Figure 2(a) shows scanning electron micrographs (SEMs) with a magnification of 50 KX of the ZnO thin film on silicon substrate. It is seen that the nanoneedles constituting the ZnO films were almost homogeneous and closely packed. The inset shows a cross-sectional view of ZnO NNs with a maximum length of  $\sim 400$  nm. The energy-dispersive x-ray (EDX) spectra of the films are shown in Fig. 2(b). The EDX analyses clearly confirm the presence of three elements, for example, Zn, O, and Al in the deposited film in addition to Si present in the substrate. The inset on the image also shows the elements (by corresponding wt. %) present in the ZnO thin films.

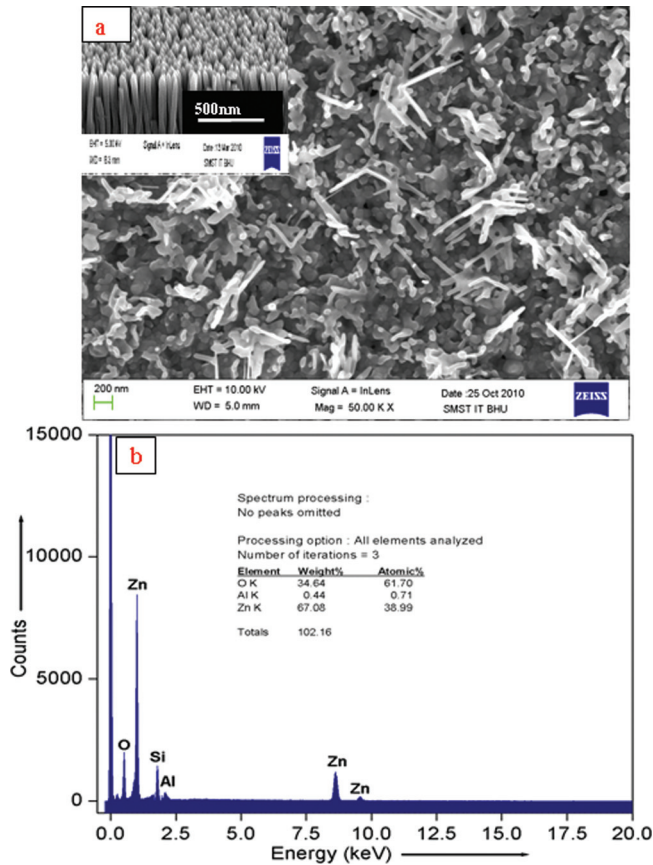


FIG. 2. (Color online) (a) SEM images of ZnO thin films on silicon substrate with 50 KX magnification. Inset shows a cross-sectional view of ZnO NNs. (b) The energy-dispersive x-ray (EDX) spectra of ZnO thin film.

## B. Characterization of Schottky nanocontact

One of the key components in this piezoelectric nanogenerator is the rectifying nanocontact between the metal electrode and individual ZnO nanoneedle. This contact serves as a switch to maintain unidirectional electrical output.<sup>2,17</sup> The contact between the Pt tip and ZnO nanoneedle is a nanoscale metal–semiconductor (M–S) Schottky contact. The nano-Schottky contacts in the present study are formed between the Pt-coated AFM tip pressed onto nanoneedles.<sup>22,23,25</sup> To examine the characteristics of individual Schottky nanocontacts to a single ZnO nanoneedle, we used the atomic force microscope in current sensing mode. A Pt (work function = 6.1 eV)<sup>17</sup>-coated Si tip was used as a nanoprobe for the measurement. Because the electron affinity of ZnO (4.5 eV)<sup>17</sup> is less than the work function of Pt, the Pt/ZnO contact behaves as a Schottky contact. Figure 3(a) shows the experimental setup used for characterizing the  $I$ - $V$  behavior of Pt tip of AFM probe/ZnO NN contact. The current through the contact was measured at various bias voltages applied between the Pt tip and an individual ZnO nanoneedle. A constant normal force of 20 nN (unless stated otherwise) was maintained between the probe tip and ZnO nanoneedle arrays in the current sensing mode. Figure 3(b) shows the experimentally measured  $I$ - $V$  characteristics for the Pt-tip/ZnO nano-Schottky contact. The  $I$ - $V$  characteristics depicted in Fig. 3(b) confirm the rectifying nature of the contact. The cut-in voltage is estimated to be 2.52 V. The current is negligibly small

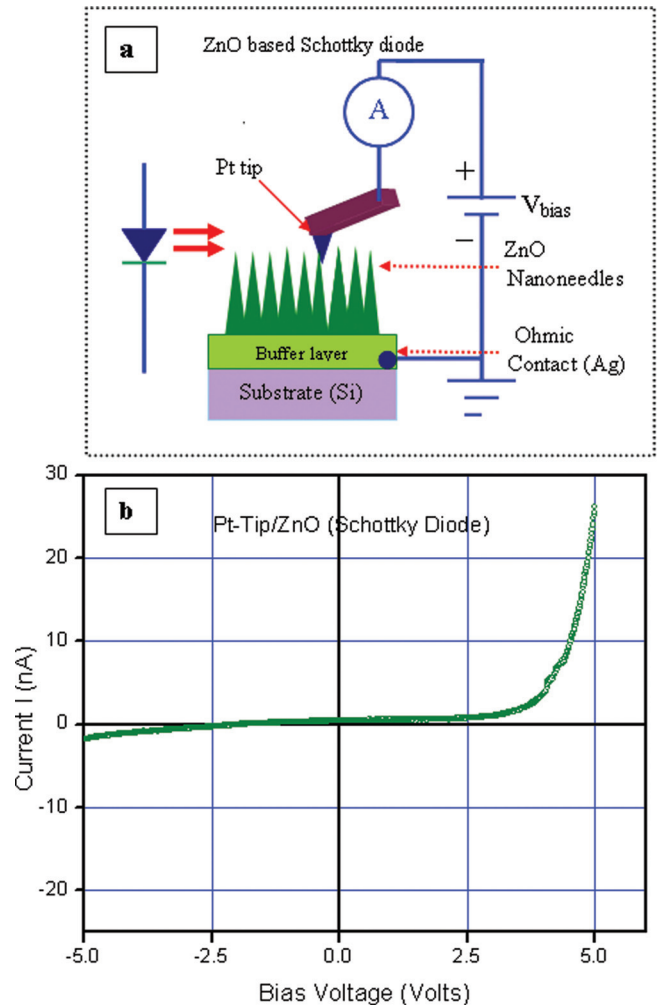


FIG. 3. (Color online) (a) Experimental setup for the  $I$ - $V$  measurement of Pt/ZnO NN contact. (b)  $I$ - $V$  characteristics of a Pt-tip/ZnO NN contact, showing rectifying behavior.

even at a moderate value of reverse voltage, demonstrating the fact that ZnO nanoneedle/Pt Schottky contact can be efficiently used as a switch for the purpose of nanopulse generation.

## C. Demonstration of nanogenerator action of ZnO NNA

Piezoelectric measurements were performed using AFM with a conducting Pt-coated silicon tip, which has a taper angle of  $20^\circ$  and radius of curvature 35 nm. The rectangular cantilever of the AFM has a spring constant of 1–2 N/m. A constant normal force of 20 nN was maintained between the tip and NN in the contact mode. To obtain an electric contact at the bottom of the NNA, silver paste was applied to connect the film on the substrate surface with the measurement circuit. A high resistance ( $R_L \sim 5 \times 10^8 \Omega$ ) was connected in series with the nanoprobe of the AFM system so that under normal condition, the measurement circuit is almost under open circuit condition. When a clean ZnO NN is bent by the atomic force microscope (AFM) tip, an asymmetric strain is produced across the width of the ZnO NN. As a result of piezoelectric effect, the stretched side of the NN develops a positive potential and its compressed side a

negative potential.<sup>17,25</sup> It is understood that the bending of a nano strand of ZnO by a conductive atomic force microscope tip causes the displacement energy from the tip to be transferred to the elastic bending energy of the nano strand.<sup>17</sup> The piezoelectric property of ZnO in turn converts this energy to electrical energy and stores it in the form of accumulated charges. The Schottky contact acts as a switch that either helps in accumulating the charge or discharging the same in the external circuit depending on the nature of the bias (reverse or forward). When a single nanoneedle is deflected laterally, the tensile side develops a positive voltage and the compressed side develops a negative voltage with respect to the substrate.<sup>17</sup> As the scanning tip touches the tensile (stretched) side of the nanoneedle, the diode gets reverse biased and the nanogenerator works in the accumulation mode. When the tip touches the compressed side, the diode gets forward biased, allowing the accumulated charge to flow through the external circuit. This is illustrated in Figs. 4(a) and 4(b) with equivalent electrical circuit representation. No external voltage was applied at any stage of the measurement

(Fig. 4). This confirms that the nanogenerator is a self power generating device that drives current through the external load by exploiting the piezopotential induced by dynamic straining.<sup>1-5</sup>

The surface morphology and the corresponding output voltage images [Fig. 5(a)] across the load were recorded simultaneously when the CAFM tip was made to scan the aligned NN arrays. Figure 5(b) is a 3D output potential image after scanning an area of  $5 \times 5 \mu\text{m}$  over the *n*-type ZnO NN array. Figure 5(a) illustrates the comparison of line scan topography image (dotted line) and the corresponding output voltage profile (solid line). The first vertical dotted line on the left-hand side of each pulse corresponds to the tip of the nanoneedle where the transition from stretching to compression occurs, while the second dotted vertical line corresponds to the occurrence of the peak of the output voltage pulse. It is seen that all the electrical pulses are negative and have an average amplitude of  $<8-9 \text{ mV}$ . Some peaks are, however, as high as  $35 \text{ mV}$ . This observation is fairly similar to that reported for

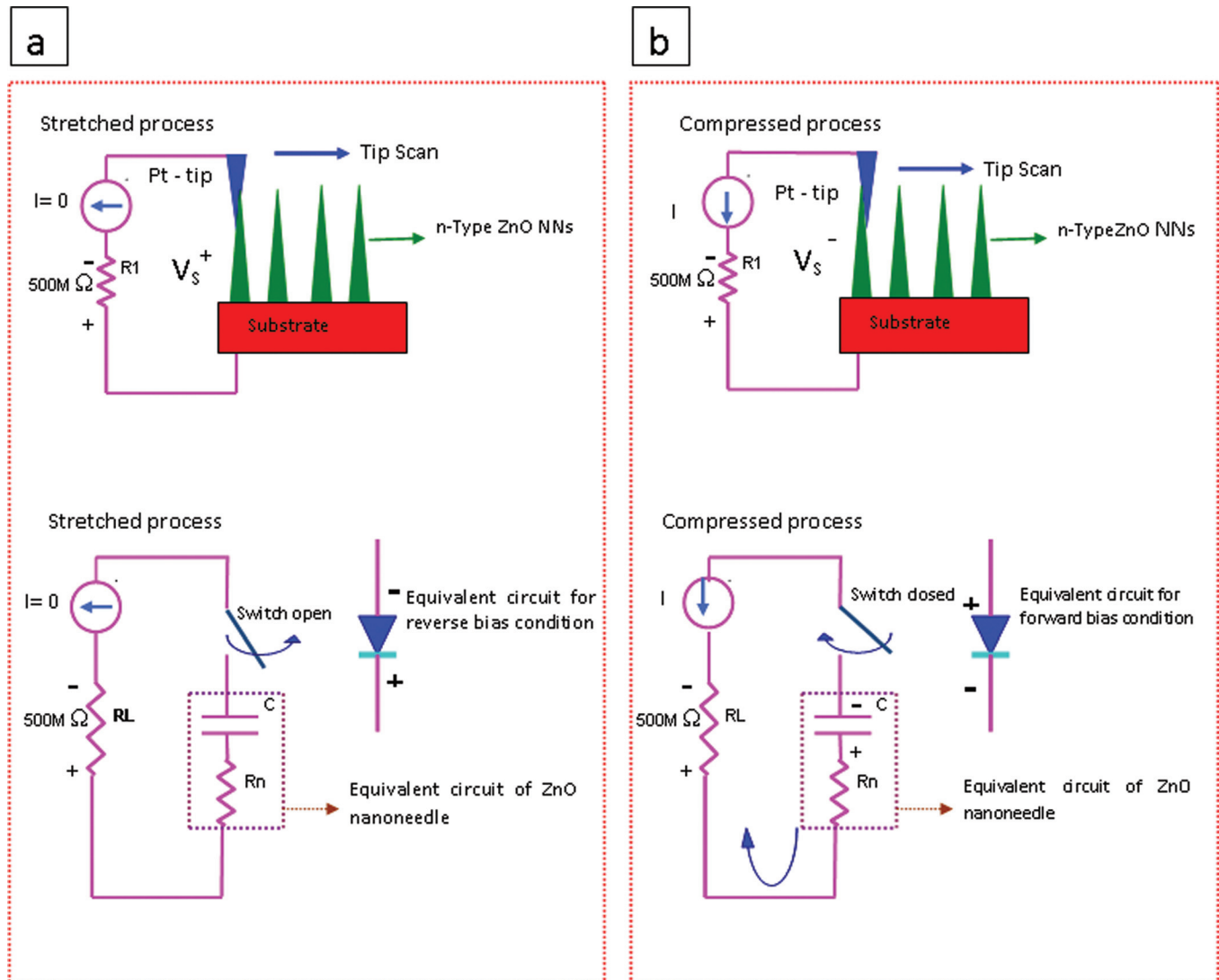


FIG. 4. (Color online) Schematic of nanogenerator principle using a conductive atomic force microscope (AFM). (a) Equivalent electrical circuit representation of reverse biased of ZnO/Pt contact under stretched condition. (b) Equivalent electrical circuit representation of forward biased of ZnO/Pt contact under compressed condition.

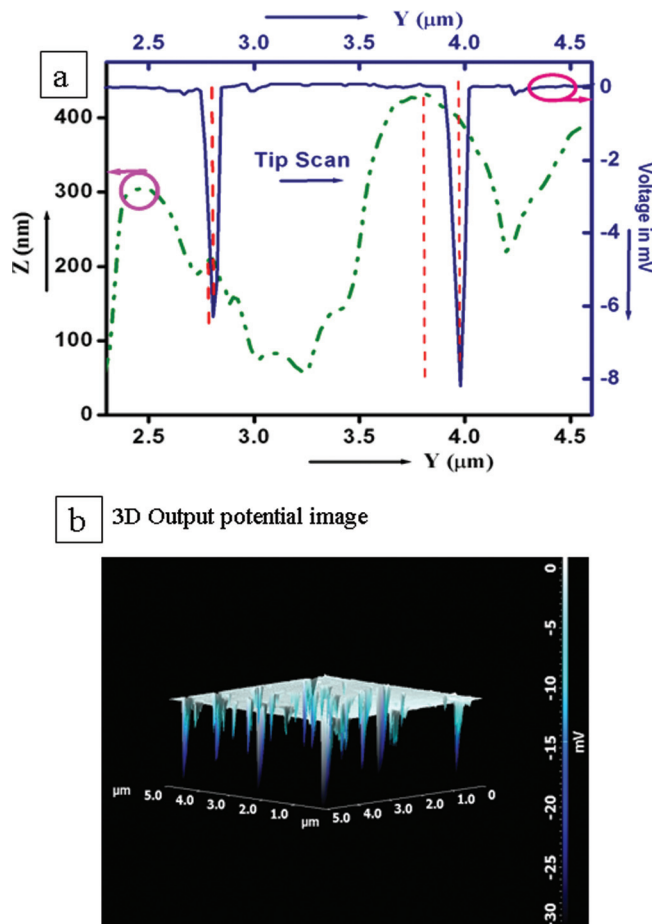


FIG. 5. (Color online) Piezoelectric power generation using the *n*-type ZnO NN arrays. (a) A typical line scan profile from the AFM topography and the corresponding output voltage images. (b) Three dimensional plot of the output voltage across the external load.

nanogenerator based on an *n*-type ZnO nanowire by Wang *et al.*<sup>17</sup> The origin of these pulses can be best understood by considering the equivalent circuits shown in Figs. 4(a) and 4(b) for the nonconducting and conducting mode of the Schottky contact switch. When the switch is in the nonconducting mode (open), the charge accumulates on the tip of the needle as shown equivalently by a capacitor. When the forward bias across the Schottky contact exceeds the cut-in voltage, the switch gets closed, and the capacitor discharges through the load under the transient condition. The transient current flowing through the external load gives rise to a pulse resembling the typical response of an RC discharging circuit. The peak amplitude of the voltage pulses depends on a number of factors including the size of the nanoneedle, the force on the AFM tip, the scanning rate, and the surface morphology of the thin film nanostructure. For a scanning rate of 1 Hz, the velocity of the scanning AFM tip is 10  $\mu\text{m/s}$ . Translating the voltage pulses in the space domain to the corresponding time domain, the full-width half-maximum (FWHM) time constant of the RC circuit is estimated to be  $\tau = (R_L + R_d + R_n) C = 0.542 \text{ ms}$  where  $R_L$ ,  $R_d$ , and  $R_n$  correspond to the load resistor, diode forward resistance, and the resistance of the nanoneedle, respectively. Ignoring the low value of the nanoneedle re-

sistance the equivalent capacitance of the strained nanoneedle can be estimated to be typically of the order of 1 pF.

The performance rating and long-term stability of the nanogenerator, however, depend on a number of parameters. In the present work, an extensive study has been carried out in this regard. To study the power generating capability of *n*-type ZnO NNA, measurements have been carried out on the same piece of ZnO NN thin film sample by changing scanning parameters of the AFM. By scanning a fixed area of  $5 \times 5 \mu\text{m}$  and counting the number of output voltage peaks and the average magnitude of the voltage peaks, we can gather some finer details about the energy generation. Figure 6(a) shows the variation of number of voltage peaks and average peak amplitude of the pulses with the scanning rate. It is seen that at a fixed contact force (20 nN), an increase in the scanning frequency (speed) causes the number of output voltage peaks and their average magnitude to increase almost linearly [Fig. 6(a)]. An increase in the number of voltage peaks and their amplitude with the increasing scanning speed may be accounted for the fact that at a low scanning rate the accumulation of the charge takes longer time and the Schottky contact switch also takes a longer time to be fully on. As a result, the

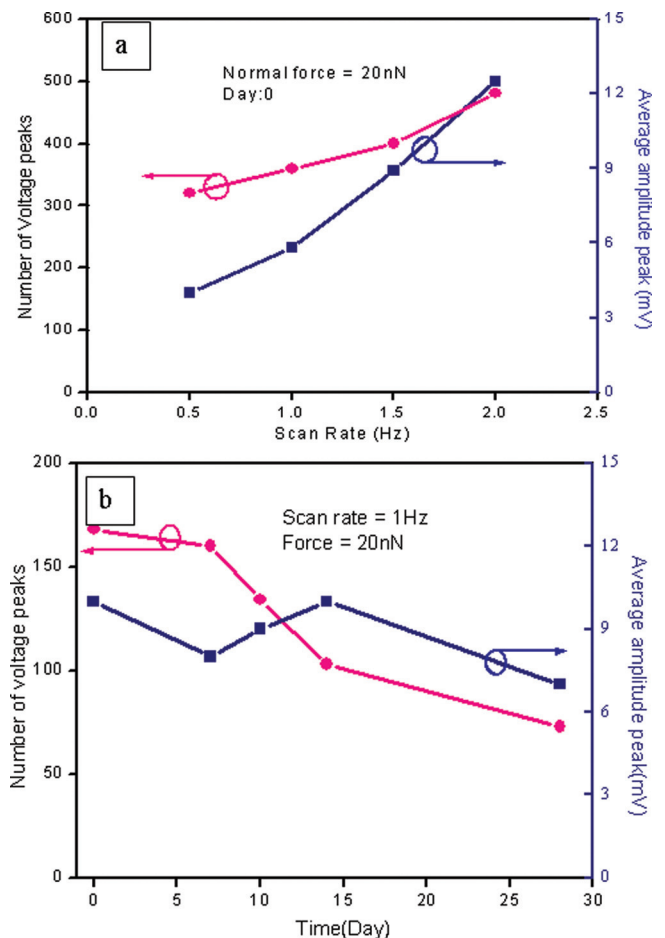


FIG. 6. (Color online) (a) The variations of the average number of voltage peaks (left axis) and the average magnitude of output voltage peaks (right axis) with AFM line scan rate. (b) Variations of the average number of voltage peaks (left axis) and the average magnitude of output voltage (right axis) as a function of post fabrication measurement instants (in days).

TABLE I. Time dependent performance of Pt/ZnO NN based nanogenerator.

Number of times scanned	Scanning Speed ( $10 \mu\text{m/s}$ )			
	Mean Value of Pulse Amplitude (mV)		Number of Electrical Pulse/( $5 \times 5 \mu\text{m}$ )	
	Normal Force (20 nN)	Normal Force (50 nN)	Normal Force (20 nN)	Normal Force (50 nN)
1	15	25	490	500
25	12	21	455	440
50	9	18	398	410

transient behavior of the nanoneedle equivalent is not observed in the case of some of the nanoneedles. On the other hand, when the scanning rate is high, the charging takes place at a fast rate, and almost all the nanoneedles exhibit the transient behavior through instantaneous charging/discharging of the equivalent capacitor. The fast scanning rate may also enable the AFM tip to reach nanoneedles of different heights as well.<sup>18</sup> We have also examined the stability of the *n*-type NNs by measuring the piezoelectric output voltage as a function of time. The second measurement was done 7 days after the sample was first fabricated and tested (day 0). The degradation in the performance was tested by making measurements on the same sample multiple of times until 28 days since its synthesis. The reduction in the number of available voltage pulses and the average peak voltage amplitudes were found to drop with time but at a much slower rate after 15 days from the date of fabrication. The performance degradation is depicted in Fig. 6(b). The further the drop in the number of output voltage pulses at the initial stage is quite significant, whereas the average peak value of voltage pulses is not affected significantly with time. This kind of rather uncorrelated behavior may be accounted for the normal wear and tear of the nanoneedle caused by the AFM tip and also the tip abrasion during the course of repeated measurements.

Among them, the normal force and scanning speed are two easily controllable parameters. They can be adjusted to optimize the output power of the nanogenerator. However, there are a number of other uncontrollable parameters, which can also vary over time and affect the output performance of the nanogenerator. Among the uncontrollable parameters, the AFM tip (other type of Schottky contacts<sup>26</sup>) abrasion seems to be the most critical one. The effect of tip abrasion on the nanogenerator output was systematically

studied by scanning the ZnO nanoneedles multiple times. The results pertaining to the preceding factors are summarized in Table I. Also 3D images of electrical output pulses of a typical sample are depicted in Figs. 7(a) and 7(b). It can be seen from Table I that the mean value of electrical pulses and the mean amplitude of electrical pulses decrease with the increasing number of scanning episodes. This is attributed to the degradation of the nano-Schottky contact, which is the key component of the nanogenerator. This degradation is partly due to abrasion of the tip because of frequent scanning. The degradation of the contact over time is also due to removal of interstitial gas ions; this is responsible for *n*-type conductivity of ZnO nanoneedles caused by repeated flexing of the nanoneedles. Repeated flexing of nanoneedles by the tip at different normal force and at larger scanning speed may cause a few of the nanoneedles to cross the elastic limit and result in a reduced piezoelectric effect in the long run.

#### IV. CONCLUSIONS

A simple and inexpensive technique has been used for demonstrating the operation of a nanogenerator using ZnO nanoneedle grown on Si substrate. The parameters that play a key role in shaping the nanogenerator pulse output have been identified. The effect of these parameters on the long-term performance of the nanogenerator has been studied in depth. The study reveals that the output of the nanogenerator can be optimized by adjusting the controllable parameters. However, the degradation of the output arising from repeated flexing of the nanostrands, wear and tear of the nanoneedles, and tip abrasion needs to be addressed for making the self power generating devices useful for future generation smart sensors.

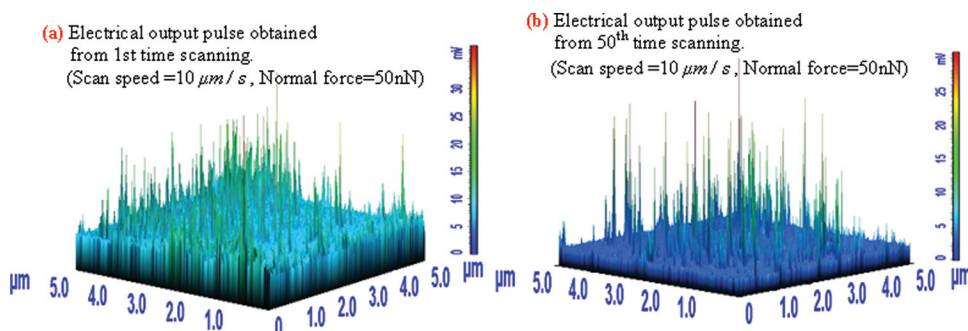


FIG. 7. (Color online) (a), (b) Comparison of the output electrical pulses obtained using different number of scanning times with constant tip normal force (50 nN) and speed ( $10 \mu\text{m/s}$ ).

## ACKNOWLEDGMENTS

The authors are thankful to the coordinator, School of Materials Science and Technology, Institute of Technology, Banaras Hindu University, for providing the experimental facilities for carrying out the work.

- <sup>1</sup>Z. L. Wang, R. Yang, J. Zhou, Y. Qin, C. Xu, Y. Hu, S. Xu, *Mater. Sci. Eng.* **R70**, 320 (2010).  
<sup>2</sup>J. Song, H. Z. Xie, W. Z. Wu, V. R. Joseph, C. F. J. Wu, and Z. L. Wang, *Nano Res.* **3**, 613 (2010).  
<sup>3</sup>S. N. Cha, J.-S. Seo, S. M. Kim, H. J. Kim, Y. J. Park, S.-W. Kim, and J. M. Kim, *Adv. Mater.* **22**, 4726 (2010).  
<sup>4</sup>G. Zhu, R. Yang, S. Wang, and Z. L. Wang, *Nano Lett.* **10**(8), 3151 (2010).  
<sup>5</sup>S. Xu, Y. Qin, C. Xu, Y. Wei, R. Yang, and Z. L. Wang, *Nat. Nanotechnol.* **5**, 366 (2010).  
<sup>6</sup>X. Chen, S. Xu, N. Yao, and Y. Shi, *Nano Lett.* **10**(6), 2133 (2010).  
<sup>7</sup>B. Sun and H. Sirringhaus, *Nano Lett.* **5**, 2408 (2005).  
<sup>8</sup>J. J. Cole, X. Wang, R. J. Knuesel, and H. O. Jacobs, *Nano Lett.* **8**, 1477 (2008).  
<sup>9</sup>S. Xu, Y. Wei, J. Liu, R. Yang, and Z. L. Wang, *Nano Lett.* **8**, 4027 (2008).  
<sup>10</sup>M. C. Newton, S. Firth, and P. A. Warburton, *Appl. Phys. Lett.* **89**, 072104 (2006).  
<sup>11</sup>J. Song, J. Zhou, and Z. L. Wang, *Nano Lett.* **6**, 1656 (2006).  
<sup>12</sup>X.W. Sun, J. Z. Huang, J. X. Wang, and Z. Xu, *Nano Lett.* **8**, 1219 (2008).  
<sup>13</sup>Y. Liu, C. Pan, Y. Dai, and W. Chen, *Mater. Lett.* **62**, 2783 (2008).  
<sup>14</sup>C. Li, Z. Du, H. Yu, and T. Wang, *Thin Solid Films* **517**, 5931 (2009).  
<sup>15</sup>J. H. He, C. L. Hsin, J. Liu, L. J. Chen, and Z. L. Wang, *Adv. Mater.* **19**, 781 (2007).  
<sup>16</sup>X. Wang, J. Zhou, J. Song, J. Liu, N. Xu, and Z. L. Wang, *Nano Lett.* **6**, 2768 (2006).  
<sup>17</sup>Z. L. Wang and J. Song, *Science* **312**, 242 (2006).  
<sup>18</sup>M. P. Lu, J. Song, M.Y. Lu, M. T. Chen, Y. Gao, L. J. Chen, and Z. L. Wang, *Nano Lett.* **9**, 1223 (2009).  
<sup>19</sup>P. X. Gao, J. Song, J. Liu, and Z. L. Wang, *Adv. Mater.* **19**(1), 67 (2007).  
<sup>20</sup>M.Y. Choi, D. Choi, M. J. Jin, I. Kim, S. H. Kim, J.Y. Choi, S. Y. Lee, J. M. Kim, and S.W. Kim, *Adv Mater.* **21**, 1285 (2009).  
<sup>21</sup>J. Song, and S. Lim, *J. Phys. Chem. C*, **111**, 596 (2007).  
<sup>22</sup>C. Periasamy, Rajiv Prakash, and P. Chakrabarti, *Mater. Sci.: Mater.Electron.* **21**, 309 (2010).  
<sup>23</sup>C. Periasamy and P. Chakrabarti, *J. Vac. Sci. Technol. B*, **27**(5), 2124 (2009).  
<sup>24</sup>W. I. Park, D. H. Kim, S. W. Jung, and G. C. Yi, *Appl.Phys.Lett.* **80**, 4232 (2002).  
<sup>25</sup>Y. Gao and Z. L. Wang, *Nano Lett.* **7**, 2499 (2007).  
<sup>26</sup>X. Wang, J. Song, J. Liu and Z. L. Wang, *Science* **316**, 102 (2007).